The Negative Gravity Field Over the 85°E Ridge

Char-Shine Liu

Geological Research Division, Scripps Institution of Oceanography, University of California, San Diego
La Jolla, California 92093

David T. Sandwell

National Geodetic Survey, National Ocean Survey, NOAA, Rockville, Maryland 20852

Joseph R. Curray

Geological Research Division, Scripps Institution of Oceanography, University of California, San Diego
La Jolla, California 92093

An isopach map made from seismic reflection and refraction data in the Bay of Bengal shows two prominent N-S trending features in the basement topography. One is the northernmost portion of the Ninetyeast Ridge which is totally buried by sediments north of 10°N. The other buried ridge trends roughly N-S for 1400 km at 85°E to the latitude of Sri Lanka and then curves toward the west. It has basement relief up to 6 km. Two free-air gravity anomaly profiles across the region show a strong gravity low (~−60 mGal) over the 85°E Ridge, while the Ninetyeast Ridge shows a gravity high. To understand the negative free-air gravity anomaly over the 85°E Ridge, we model the lithosphere as a thin elastic plate and calculate its flexural and gravitational response to an uneven sediment load. A plausible formation history for a buried ridge consists of at least two major episodes. The first is the formation of the ridge on a lithosphere with a flexural rigidity of D_1. At some later time the ridge is buried by an influx of sediments, the lithosphere is cooler, and the flexural rigidity has increased to D_2. The character of the gravity field depends primarily upon the initial and final values of flexural rigidity. These D_1 and D_2 values are varied to obtain good agreement between the model and observed gravity anomalies. Best fitting models have a 180 times increase in flexural rigidity between ridge formation and sediment burial. An approximate relationship between flexural rigidity and crustal age shows that the 85°E Ridge was formed on relatively young lithosphere, 5-15 m.y. old and that it was buried when the lithosphere was 40-80 m.y. old.

INTRODUCTION

The relationship between gravity and topography is commonly used to infer the compensation mechanism for large topographic features such as seamounts and aseismic ridges. Since the asthenosphere cannot maintain large deviatoric stresses over geologic time [*Heiskanen and Vening Meinesz*, 1958], the load of a seamount must be supported by stresses within the lithosphere. These stresses can be distributed either directly beneath the load point (local compensation) or in a region surrounding the point of loading (regional compensation). The gravity field is sensitive to the spacial distribution of compensating masses and therefore can be used to discriminate between locally and regionally compensated topography. To make this distinction, however, a compensation model must be introduced.

A Pratt-type compensation model has been used to explain the gravity field over the Ninetyeast Ridge between the equator and 5°S [*Bowin*, 1973], while the Airy-type model is used to explain the gravity data over the eastern Walvis Ridge [*Goslin and Sibuet*, 1975]. There-

fore it appears that these two aseismic ridges are locally compensated. However, the gravity field of other aseismic ridges can best be explained by regional compensation models. Commonly used models consist of an elastic, elastic-plastic, or viscoelastic plate overlying an incompressible fluid half space [*Turcotte*, 1979]. In the elastic plate model, the lithospheric strength is specified by a flexural rigidity or effective elastic thickness (EET). This model can explain the gravity field and flexural topography of the Hawaiian-Emperor Seamount Chain [*Vening Meinesz*, 1941; *Gunn*, 1943; *Walcott*, 1970; *Watts and Cochran*, 1974; *Watts*, 1978], the Walvis Ridge [*Kogan*, 1976; *Detrick and Watts*, 1979], and the Ninetyeast Ridge between about 25°S and the equator [*Detrick and Watts*, 1979]. The EET's inferred from the studies at both the Walvis Ridge and Ninetyeast Ridge are close to zero, indicating that these two ridges are locally compensated since the elastic plate model with zero EET is equivalent to the Airy compensation model. However, the EET of the lithosphere along the Hawaiian-Emperor Seamount Chain varies from about 30 km at the island of Oahu in the southeast, to 10 km at Jimmu Seamount in the northwest [*Watts*, 1978]. It has been shown that these large variations in lithospheric strength are correlated with the age of the lithosphere at the time of loading [*Watts*, 1978]. Studies of lithospheric flexure at subduction zones confirm

this first-order relationship between EET and age [*Caldwell and Turcotte*, 1979]. More recent studies demonstrate that the strength of the lithosphere also depends upon the magnitude of the load [*McNutt and Menard*, 1982]. However, the strength-age dependence is usually dominant and basically reflects the age-dependent thermal structure of the lithosphere and the strong temperature dependence of the creep processes which tend to relieve flexural stresses [*Bodine et al.*, 1981].

Both the local and regional compensation models predict that the ratio of free-air gravity anomaly to seafloor topography is positive at short wavelengths. For example, the gravity anomaly over a seamount that is Airy compensated results from two mass anomalies. The topography is a positive surface mass which produces a positive gravity field; the compensating mass at depth, which is equal and opposite to the surface mass, produces an negative gravity field. The observer on the sea surface is closer to the positive mass than the negative mass and therefore records a positive gravity anomaly. The same geometric effect occurs for regionally compensated topography, although the situation is more complex since not all of the compensating mass lies directly beneath the seamount. Thus it appears that the free-air gravity anomaly is always positive above the crest of a ridge. In this paper, we present an exception to this rule and demonstrate that this exceptional behavior fits neatly into the framework of the regional compensation models with age-dependent EET.

Curray and Moore [1971, 1974] and *Curray et al.* [1982], using seismic reflection and refraction data, have described a N-S trending aseismic ridge in the Bay of Bengal at about 85°E, the northern part of which is completely buried by a thick layer of sediments (>6 km). The southern part of the 85°E Ridge curves around toward the west and locally outcrops above the sediments of the Bengal Fan as a series of seafloor hills. While the location and amplitude of this ridge are fairly well constrained, nothing is known about its age, formation history, and lithology. One clue lies in its unique gravity field which is strongly negative (e.g., −60 mGal) directly over the crest of the northern part of the ridge. Perhaps the simplest explanation for the gravity low is that the ridge is less dense than the adjacent sediments [*Curray et al.*, 1982]. However, the strong magnetic signal over the northern part of the ridge as well as its great length and amplitude indicate that it is similar to other linear aseismic ridges. The major question is: Why is the gravity field of this 85°E Ridge so dissimilar to other aseismic ridges? The only other major difference between this ridge and other aseismic ridges is that the northern part of the 85°E Ridge is completely buried by sediments. Thus the sediment load may have a strong influence upon the gravity field.

To estimate the effects of sediment loading, we present some constraints on the formation history for this buried ridge. We model the oceanic lithosphere as a thin elastic plate overlying an incompressible, inviscid fluid half space and calculate its flexural and gravitational response to the load of a linear ridge. We then increase the lithospheric flexural rigidity to account for the stiffening of the lithosphere during the time interval between ridge formation and sediment burial. Finally, we bury our model ridge by sediments and calculate the gravitational response to this second load. We will show that if the flexural rigidity of the lithosphere increases with age, then the sediment loading drastically changes the gravitational field from a large positive free-air gravity anomaly over the ridge to a strong negative value. By fitting the predicted gravity anomaly from this two-step loading model to the observed gravity field over the 85°E Ridge, we are able to estimate both the flexural rigidity at the time the ridge was formed and the flexural rigidity at the time of sediment loading. Finally, using the flexural rigidity-age relationship derived from previous studies, we estimate the timing of the two loading events.

THE 85°E RIDGE

The 85°E Ridge in the Bay of Bengal (northeastern Indian Ocean) is covered in its northern portion by the Bengal Deep-Sea Fan, the largest deep-sea fan in the world [*Curray and Moore*, 1971, 1974; *Moore et al.* 1974]. As shown in Figure 1, the fan extends from the continental shelf in the north, where the sediment thickness exceeds 16 km, to about 5°S, where the sediments pinch out. The bathymetry of the region is extremely smooth with a gentle north to south gradient, reflecting the northward increasing sediment thickness and southerly transport of the turbidities comprising the fan. An isopach map of the region (Figure 2) was constructed from seismic reflection and refraction data by *Curray et al.* [1982]. The isopach contours show two N-S trending highs in the basement topography. The eastern buried ridge is the northern end of the Ninetyeast Ridge, which lies close to the Sunda Trench and is currently being subducted at its northern extreme [*Curray et al.*, 1982]. The 85°E Ridge trends roughly N-S between latitudes of 5°N and 17°N; south of 5°N it turns toward the southwest and west. The overall known length of this ridge is greater than 1600 km.

A free-air gravity anomaly map (Figure 3) for this same region was constructed by Liu and Emmel using all the available data collected from various Scripps , Lamont, and NOAA cruises. The free-air gravity field reflects many of the N-S trending features that appear in the isopach map (Figure 2), including the 85°E Ridge, the Ninetyeast Ridge, and the Sunda Trench.

The isopach and free-air gravity maps of Figures 2 and 3 reveal some basic characteristics of the 85°E Ridge.

1. The length of the ridge is much greater than its width (i.e., it can be modeled as a two-dimensional feature).

2. The amplitude of the basement topography is greater than 4 km between latitudes of 10°N and 15°N.

3. The gravity anomaly of the ridge has a relative low, and it is surrounded by two relative highs.

These basic features are constrained from many geophysical profiles [*Curray et al.*, 1982, Figure 3]. To investigate the 85°E Ridge in greater detail, we will use primary geophysical data from two profiles crossing the most prominent portion of the 85°E Ridge in the E-W directions. The locations of these profiles T53-54, at about 13°N, and T6-11, at 10°N, are shown in Figure 3.

DATA

Underway geophysical data including 3.5-KHz bottom-pennetrating echo sounding, scalar magnetics, and con-
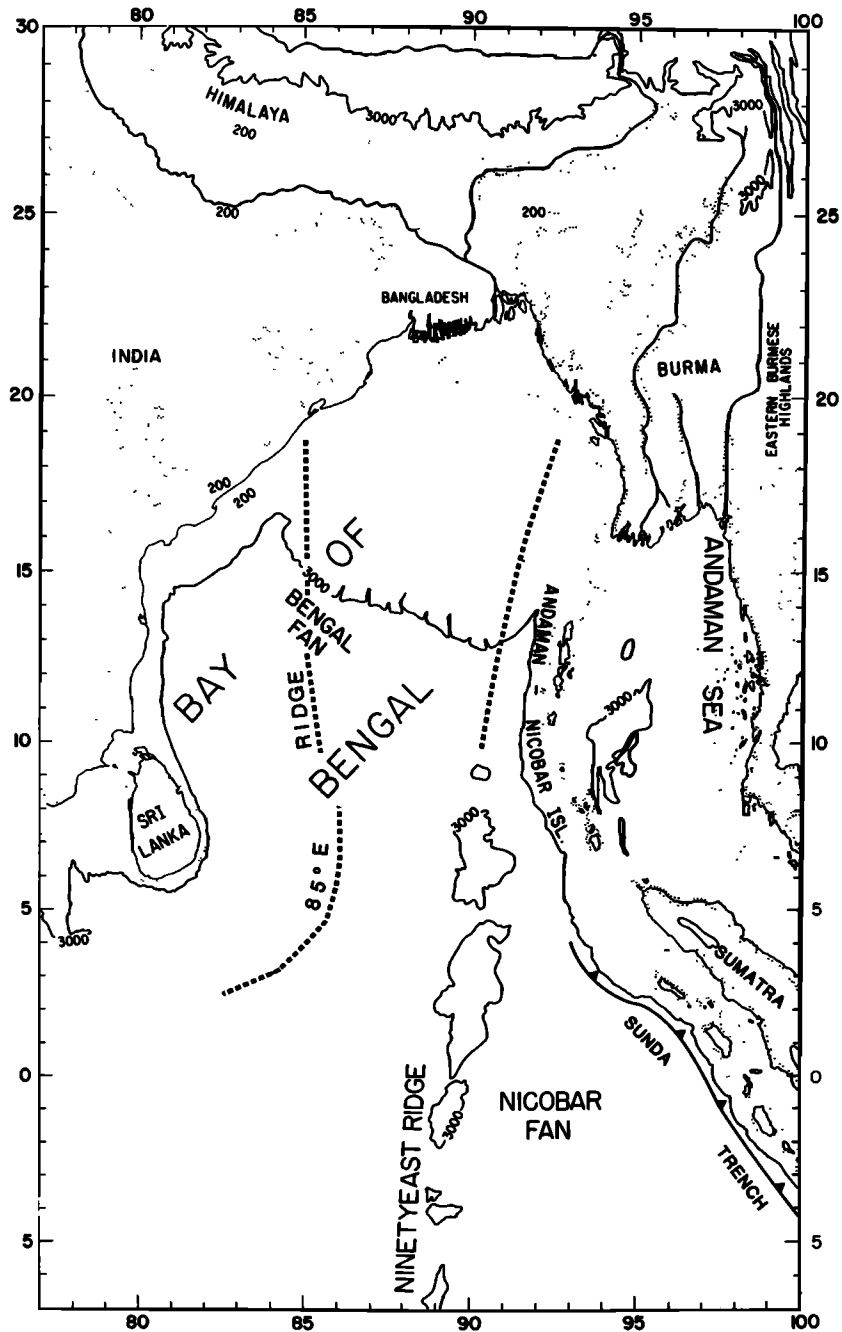
Fig. 1. Map of the Bay of Bengal shows the prominent tectonic features of the region including the Indian continent, the Ninetyeast Ridge, and the Sunda Trench. The locations of the 85°E Ridge and the northernmost portion of the Ninetyeast Ridge are indicated by dashed lines; they are completely buried by sediments [after *Curray et al.*, 1982].

tinuous seismic reflection data have been collected during many cruises of the Scripps Institution of Oceanography vessels in the Bay of Bengal. Gravity data have been collected along tracks T53-54 and T6-11, and a large number of seismic refraction lines were also run. Basement depth models along each of these tracks were constructed from the available seismic information, although generally, the reflection data did not penetrate to sufficient depth to constrain the basement topography. Seismic reflection data along many profiles, including T53-54 and T6-11, and velocities derived from wide-angle reflection and refraction data were used to map major unconformities [*Curray et*

al., 1982]. A Paleocene-Eocene unconformity, labeled P in Figures 4 and 5, appears in the reflection data and clearly delineates the location of the 85°E Ridge. The P unconformity is anomalously shallow in profile T53-54 at about 85°E. Based upon this rather abrupt upwarping, we believe that the crest of the 85°E Ridge lies directly beneath the P unconformity, as shown in our basement model in Figure 4. The crest of the 85°E Ridge can be seen in the reflection data in line T6-11 (Figure 6). From the pattern of the reflectors, it appears that the major portion of the 85°E Ridge lies 30-40 km eastward of the basement peak. We have included this effect in our basement model in
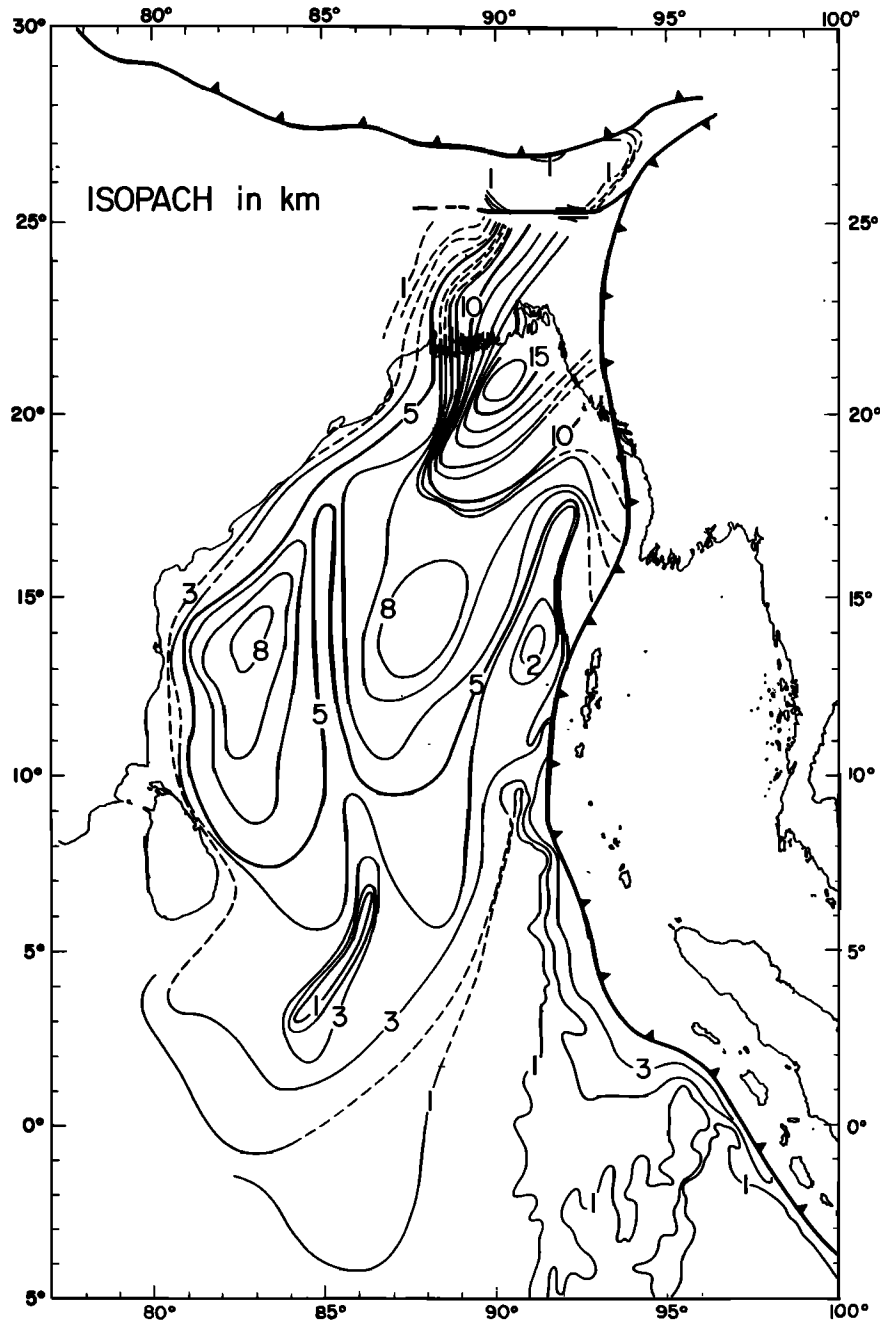
Fig. 2. Isopach map of the Bengal Deep-Sea Fan. The seafloor in this region is very smooth. Variations in sediment thickness correspond to undulations in the basement topography [after *Curray et al.,* 1982].

Figure 5. The shallower unconformities along each of the profiles reflect compaction and slumping of the thick sediments adjacent to the 85°E Ridge and the Ninetyeast Ridge. Where the basement topography was not constrained by any data, we performed a linear interpolation between points, except near the 85°E Ridge, where we constructed a basement model to reflect the undulations in the P unconformity. The sediment thickness is 6-8 km along profile T53-54 on either side of the 85°E Ridge, while over the crest of the ridge the sediments are only about 2 km thick. Profile T6-11 lies approximately 300 km to the south of profile T53-54. In this region the sediments are thinner (4-5 km in thickness), and the 85°E

Ridge is apparently somewhat lower. Since we will use these basement models to construct model gravity fields, we will show that the more speculative aspects of the models have little effect upon our final results and conclusions.

The free-air gravity anomaly along each of these profiles is shown in the center of Figures 4 and 5. To remove the regional gravity field, we have constructed a long-wavelength gravity anomaly profile from the low degree and order spherical coefficients (i.e., $l, m \leq 10$) of the Goddard Earth Model 10 [*Lerch et al.,* 1979] and subtracted this regional field from the observed anomalies. The remaining gravity anomalies, from west to east along
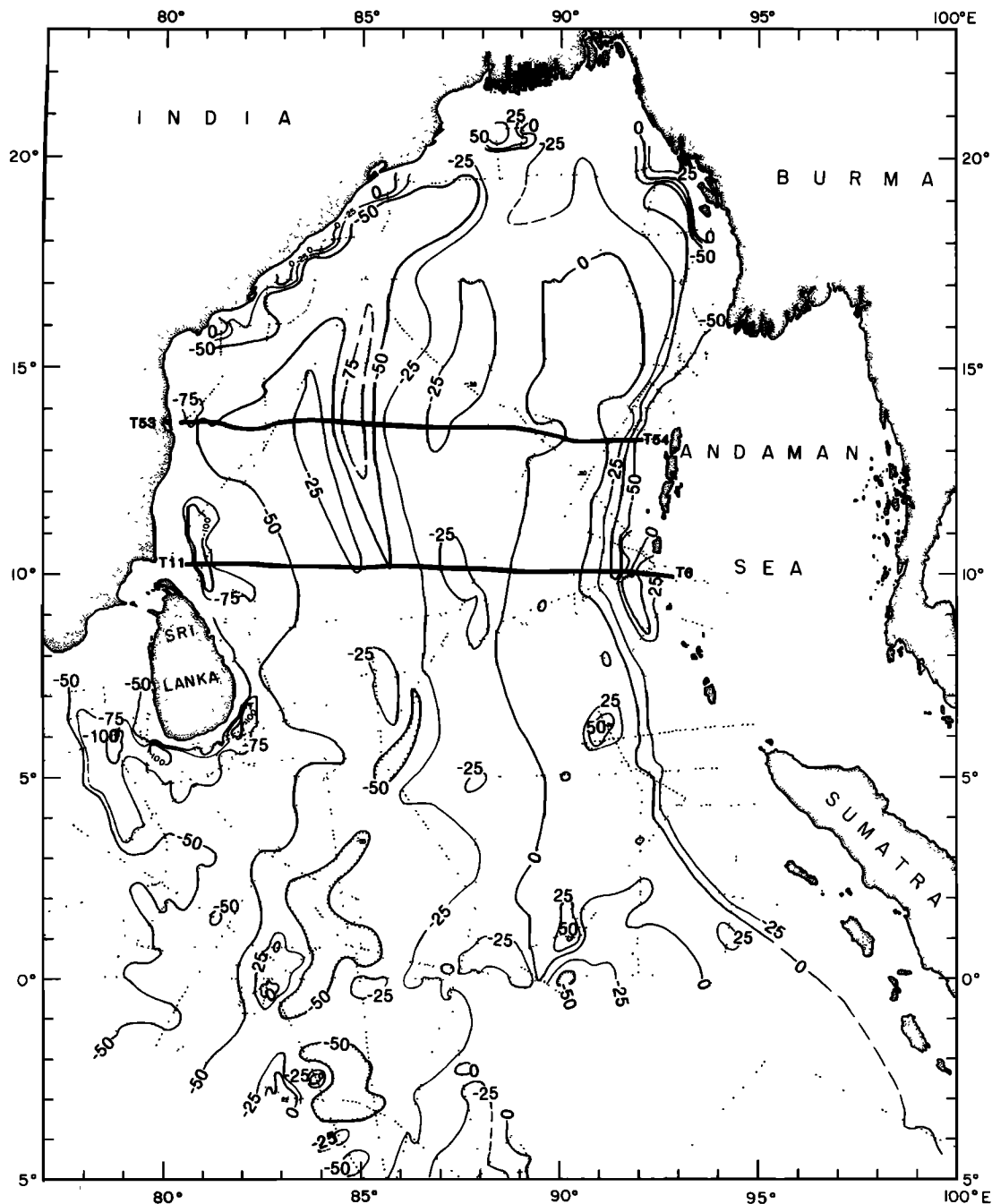
Fig. 3. Free-air gravity anomaly map of the Bay of Bengal. Dotted lines indicate the surface ship gravity measurements. Ship's tracks T53-54 and T6-11 are shown in heavy lines. The outstanding gravity anomalies are the lineated negative anomaly running N-S at about 85°E and the positive anomaly over the Ninetyeast Ridge.

each profile, show the continental edge effect of the Indian continental shelf, a prominent gravity low at the 85°E Ridge, which is surrounded by two smaller relative highs, a gravity high over the Ninetyeast Ridge, and a sharp gravity low at the Sunda Trench. It is notable that the Ninetyeast Ridge is associated with a relative gravity high while, the 85°E Ridge has a gravity low. The difference between the gravity signal of these two ridges can be explained by their respective distances from the Sunda Trench. The northern portion of the Ninetyeast Ridge is superimposed upon the outer swell of the Sunda Trench [*Curray et al.*, 1982]. Typically, the outer rise associated

with a subduction zone produces a broad belt (200-500 km) of positive gravity anomalies (30-60 mGal) seaward of the trench axis [*Watts and Talwani*, 1974]. Figure 3 shows that a similar belt of relative positive gravity anomaly appears seaward of the Sunda Trench axis. This outer swell gravity high may dominate or cancel any of the gravity effect of the Ninetyeast Ridge. On the other hand, the outer swell gravity high has a negligable effect upon the gravity field of the 85°E Ridge since the ridge lies more than 600 km from the trench axis. The 85°E Ridge is also far enough from the Indian continental margin to be largely uneffected by the continental gravitational edge
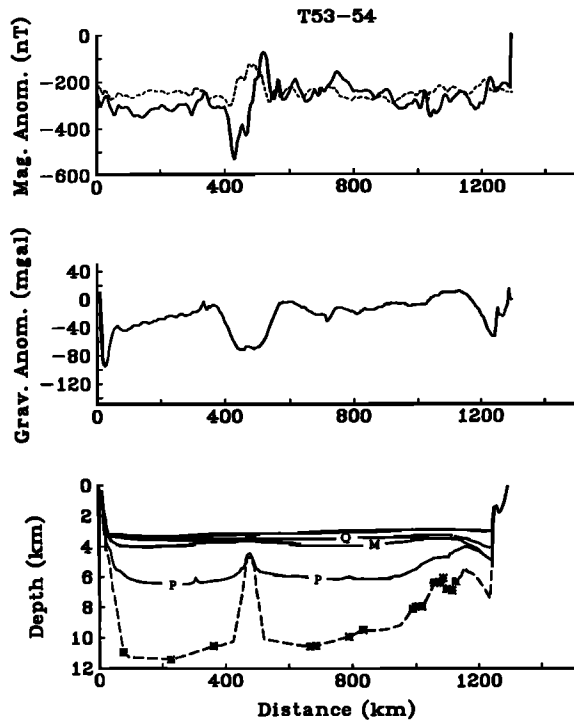
Fig. 4. Geophysical data for track T53-54. (bottom) Dashed line indicates the basement topography derived from refraction stations (asterisks) and reflection data over the peak of the 85°E Ridge at about 470 km. Q, M, and P are interpreted isochrons of base of the Quaternary, an upper Miocene unconformity, and a Paleocene-Eocene unconformity [Curray et al., 1982]. (center) The dip in the free-air gravity anomaly coincides with the axis of the 85°E Ridge. (top) The largest magnetic signal occurs over the 85°E Ridge. The deskewed magnetic anomaly profile (dashed line) is obtained by applying an inverse phase filter with $\theta = 90°$.

effect. Therefore, we believe the gravity field over the 85°E Ridge is influenced by only the ridge and its compensating mass.

To illustrate the 85°E Ridge further, the magnetic anomalies along each of these profiles are shown on the top of Figures 4 and 5. Along profile T53-54, there is a asymmetrical magnetic signal over the 85°E Ridge. A somewhat smaller signal appears along profile T6-11 over the 85°E Ridge. The overall strength of these two signals, especially for profile T53-54, indicates that the ridge is composed of highly magnetized rock. The magnetic anomaly patterns are asymmetric about the ridge because of the phase shift produced by the northward drift of the Indian plate [MacKenzie and Sclater, 1971; also see Schouten, 1971]. By applying an inverse phase filter [Schouten and McCamy, 1972] we can remove this skewing effect. The deskewed magnetic anomaly profiles are shown as dashed lines at the top of the Figures 4 and 5.

Based upon the isopach map of Figure 2, the basement models of Figures 4 and 5, and the magnetic profiles, it appears that the 85°E Ridge is similar to other aseismic ridges. However, the gravity data do not substantiate this hypothesis. In the next section, we develop a two-stage loading model to demonstrate that sediment load changes the gravity anomaly over the ridge from positive to negative values.

MODEL

Like other regional compensation models, our model lithosphere is composed of a thin elastic plate overlying an inviscid fluid half space [Walcott, 1970]. Initially, the flat seafloor is covered by a water layer with a density ρ_w and a thickness of s. The crust, of density ρ_c, has a constant thickness d, the Mohorovičić discontinunity (Moho) lies at a depth $d+s$. The remainder of the lithosphere has density ρ_m and lies at depths greater than $d+s$. Rather than define an effective elastic thickness, we will describe the initial elastic layer by a flexural rigidity D_1.

This model lithosphere is loaded by a seamount (i.e., any form of seafoor topography) of density ρ_c, with an initial elevation of $h_o(\mathbf{x})$ as shown in Figure 7a, where the vector $\mathbf{x} = (x, y)$. Since the lithosphere is elastic, it immediately flexes under the seamount load by an amount $w(\mathbf{x})$. The remaining seafloor topography $h(\mathbf{x})$, measured positive upward from the average depth s, is

$$h(\mathbf{x}) = h_o(\mathbf{x}) + w(\mathbf{x}) \tag{1}$$

The flexural deflection $w(\mathbf{x})$ is determined from the biharmonic equation for a thin elastic plate overlying a fluid half space:

$$D_1 \nabla_h{}^4 w(\mathbf{x}) = p(\mathbf{x}) \tag{2}$$
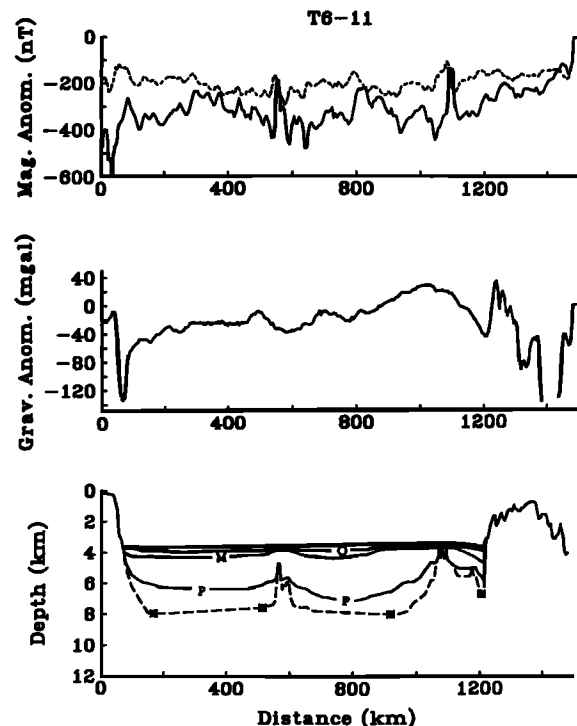
subject to the boundary condition

Fig. 5. Geophysical data for track T6-11. (bottom) The 85°E Ridge at 550 km appears in the reflection record shown in Figure 6. Other symbols are the same as in Figure 4. (center) The gravity anomaly over the 85°E Ridge is negative and is surrounded by two relative highs. (top) The 85°E Ridge is associated with a small magnetic signal. The deskewed magnetic profile (dashed line) is obtained by applying an inverse phase filter with $\theta = 85°$.
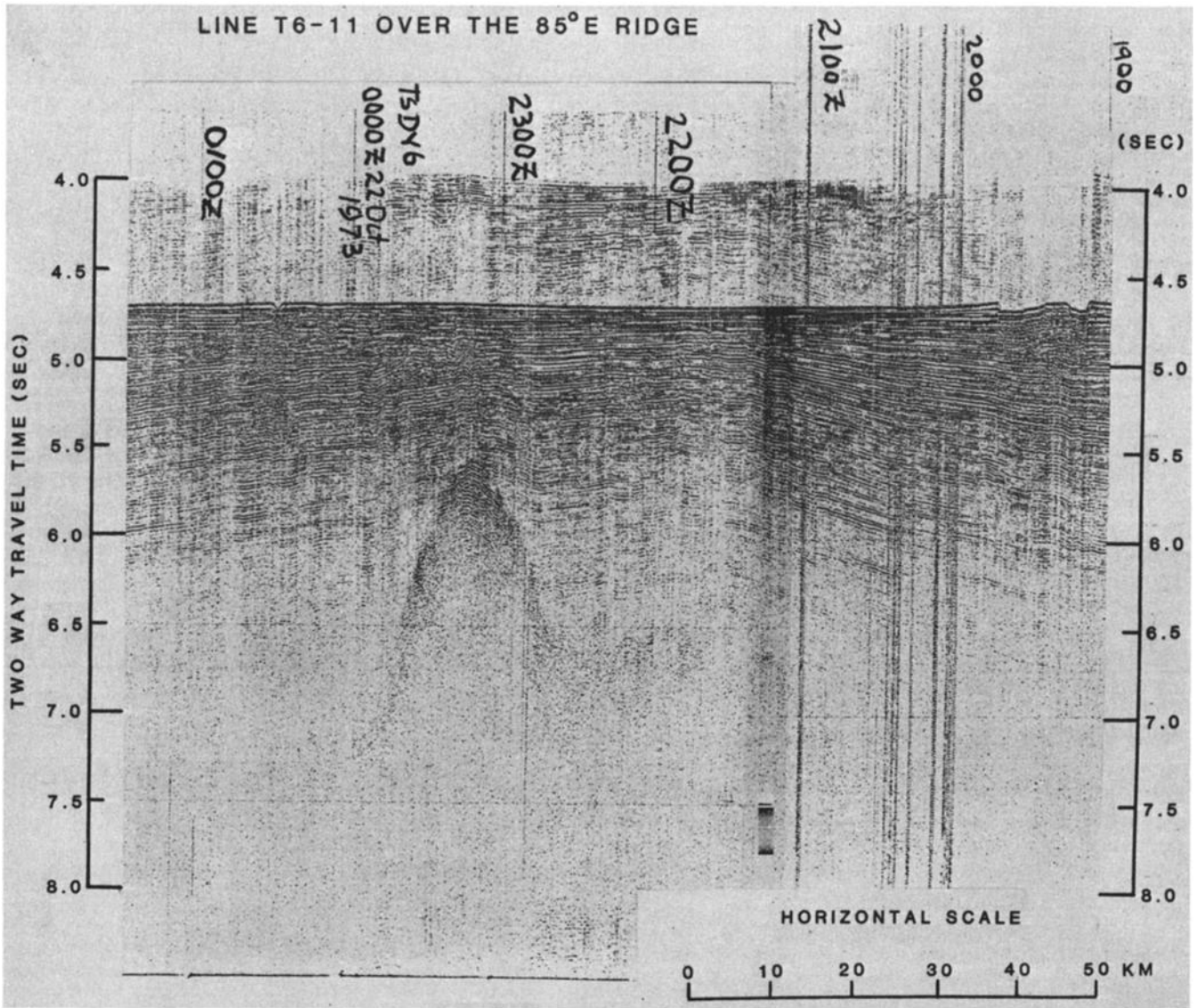
Fig. 6. Seismic reflection record along track T6-11. The peak of the 85°E Ridge appears at 2300Z (UT). The general shape of the upper reflectors indicates the main portion of the ridge lies 30-40 km to the east (right) of the ridge crest.

$$\lim_{|\mathbf{x}|\to\infty} w(\mathbf{x}) = 0 \qquad (3)$$

where

$$\nabla_h{}^4 = \frac{\partial^4}{\partial x^4} + \frac{\partial^4}{\partial y^4} \qquad (4)$$

and $p(\mathbf{x})$ is the pressure (positive upward). For a similar derivation see *Banks et al.* [1977]. The pressure is composed of surface load and restoring force

$$p(\mathbf{x}) = -(\rho_c - \rho_w)gh_o(\mathbf{x}) - (\rho_m - \rho_w)gw(\mathbf{x}) \qquad (5)$$

where g is the gravitational acceleration. After inserting (5) into (2) and Fourier transforming (2) in the $\hat{x}$ and $\hat{y}$ directions, we find

$$D_1|\mathbf{k}|^4 W(\mathbf{k}) = -(\rho_c - \rho_w)gH_o(\mathbf{k}) - (\rho_m - \rho_w)gW(\mathbf{k}) \qquad (6)$$

where the vector wavenumber $\mathbf{k} = (k_x, k_y)$ and the following Fourier transform convention is used:

$$W(\mathbf{k}) = \int_{-\infty}^{\infty}\int_{-\infty}^{\infty} w(\mathbf{x})\, e^{-i\mathbf{k}\cdot\mathbf{x}}\, dx\, dy \qquad (7)$$

$$w(\mathbf{x}) = \frac{1}{(2\pi)^2}\int_{-\infty}^{\infty}\int_{-\infty}^{\infty} W(\mathbf{k})\, e^{i\mathbf{k}\cdot\mathbf{x}}\, dk_x\, dk_y \qquad (8)$$

Since h_o cannot be measured directly, we eliminate it from (6) by using the Fourier transform of (1) and solve for the deflection of the Moho:
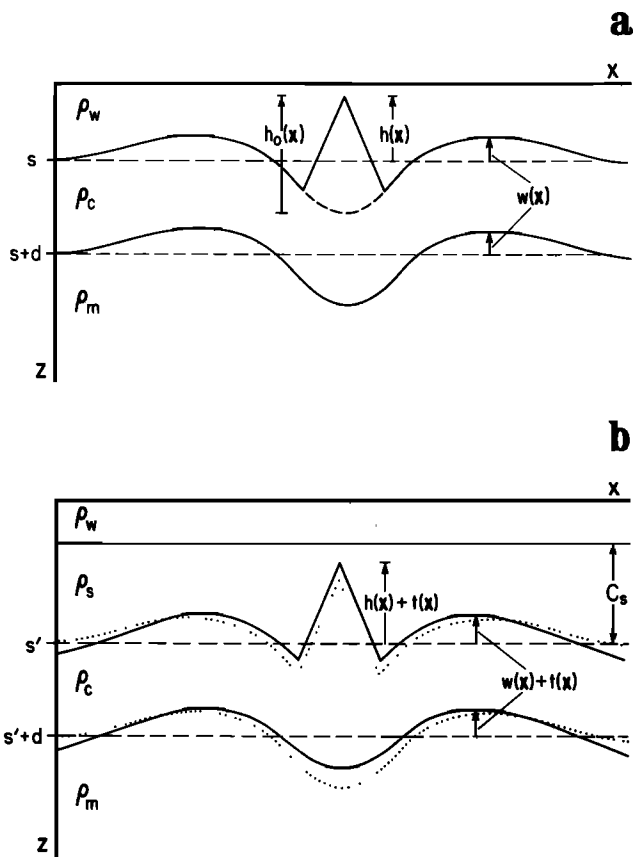
Fig. 7. (a) The model represents an elastic lithosphere overlying a fluid half space that has deflected an amount $w(x)$ under the load of a seamount. After loading, the seafloor topography is $h(x)$ = $h_o(x)$ + $w(x)$. (b) The seafloor topography is buried under a layer of sediments (density ρ_s) with an average thickness C_s. The uneven loading produces a second flexural deflection $f(x)$. The final basement topography (solid line) is the sum of the original topography $h(x)$ (dotted line) and the second flexural deflection $t(x)$.

$$W(\mathbf{k}) = -R_1(|\mathbf{k}|) \frac{(\rho_c - \rho_w)}{(\rho_m - \rho_c)} H(\mathbf{k}) \qquad (9)$$

where

$$R_1(|\mathbf{k}|) = \left[1 + \frac{D_1 |\mathbf{k}|^4}{g(\rho_m - \rho_c)} \right]^{-1} \qquad (10)$$

Banks et al. [1977] have shown that this solution satisifies the boundary condition (3).

The gravity field for the model shown in Figure 7a is most easily determined from an infinite series of nonlinear functionals [*Dorman and Lewis,* 1974; *Parker,* 1973]. For our model we use only the first term in the series; thus the Fourier transform of the gravity anomaly $G(\mathbf{k})$ is

$$G(\mathbf{k}) = 2\pi G \ e^{-|\mathbf{k}|s}\left[(\rho_c - \rho_w)H(\mathbf{k})\right.$$

$$\left. + (\rho_m - \rho_c) W(\mathbf{k}) \ e^{-|\mathbf{k}|d}\right] \qquad (11)$$

This is a good approximation when the characteristic wavelength of the topography is much greater than the topographic amplitude. This approximation, along with (9), yields an isotropic linear relationship between the Fourier transform of the gravity anomaly $G(\mathbf{k})$ and the seafloor topography $H(\mathbf{k})$:

$$G(\mathbf{k}) = Q_1(|\mathbf{k}|) \ H(\mathbf{k}) \qquad (12)$$

where the gravity/topography transfer function is

$$Q_1(|\mathbf{k}|) = 2\pi G(\rho_c - \rho_w)e^{-|\mathbf{k}|s}\left[1 - R_1(|\mathbf{k}|)e^{-|\mathbf{k}|d}\right](13)$$

Figure 8a shows the gravity/topography transfer function Q_1 for zero flexural rigidity (dashed line), which corresponds to Airy compensation, and for a flexural rigidity $D_1 = 1.8 \times 10^{21}$ N m (solid line). The important length scales, indicated in Figure 8a, are λ_s (2π times the mean seafloor depth), λ_d (2π times the Moho depth), and λ_{f1} (the flexural wavelength). The flexural wavelength is related to the flexural rigidity D_1 by
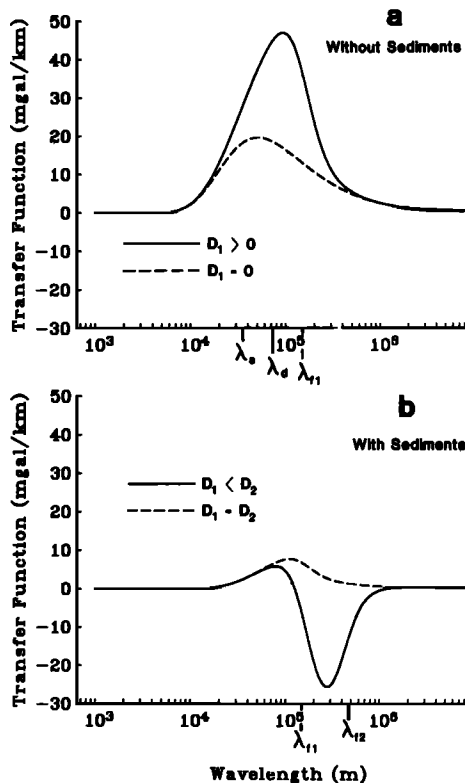

Fig. 8. (a) Gravity/seafloor topography transfer function for Airy compensated topography (dashed line) and regionally compensated topography (solid line, $D_1 = 1.8 \times 10^{21}$ N m). The important wavelengths are $\lambda_s = 35$ km, $\lambda_d = 72$ km, and $\lambda_{f1} = 152$ km. (b) Gravity/basement topography transfer function for regionally compensated topography (flexural rigidity D_1, flexural wavelength $\lambda_{f1} = 152$ km) followed by sediment burial (flexural rigidity D_2, flexural wavelength $\lambda_{f2} = 471$ km). The transfer function is positive at all wavelengths when $D_1 = D_2 = 1.8 \times 10^{21}$ N m (dashed line) and is negative for $\lambda > \lambda_{f1}$ when $D_2 = 3.2 \times 10^{23}$ N m > $D_1 = 1.8 \times 10^{21}$ N m.

$$\lambda_{f1} = 2\pi \left[\frac{D_1}{g(\rho_m - \rho_c)} \right]^{1/4} \qquad (14)$$

The peak in the Airy compensation transfer function (dashed line) lies between wavelengths of λ_d and λ_s. For nonzero flexural rigidity (solid line) the peak lies between λ_{f1} and λ_s. In both cases the gravity/topography ratio is positive for all wavelengths.

In contrast, the ratio of gravity to basement topography is negative over the crest of the 85°E Ridge. To explain the observed negative ratio of gravity to basement topography, we bury our model ridge by sediments with density $\rho_s < \rho_c$ (see Walcott [1972] for sediment loading on a continental margin). The buried ridge is shown in Figure 7b. We assume that the sediment burial occurred some time after the ridge was formed; during this time interval the lithosphere has cooled and increased in flexural rigidity to a value of D_2. The average sediment thickness is C_s. However, the sediments are thinner over the crest of the ridge than they are on the flanks of the ridge. This uneven sediment load produces both an increase in average basement depth Δs and a second flexural deflection $t(x)$. In reality, sediment loading is a continuous process. Once the ridge is completely buried, further sediment influx will tend to fill the low lying areas caused by the second flexural deformation, and the new seafloor will be flat. The sediment thickness at any point x is

$$C_s - h(x) - t(x) \qquad (15)$$

and the sediment overburden pressure $p_s(x)$ is

$$p_s(x) = -g(\rho_s - \rho_w)[C_s - h(x) - t(x)] \qquad (16)$$

When the lithosphere deflects under the sediment load, all density interfaces, including the sediment/water interface, deflect by an amount $t(x) - \Delta s$. This deflection produces a restoring pressure $p_t(x)$ of

$$p_t(x) = -g(\rho_m - \rho_w)(t(x) - \Delta s) \qquad (17)$$

The second flexural response is determined from the Fourier transform of the biharmonic equation where the pressure is the sum of (16) and (17):

$$D_2|k|^4[T(k) - \delta(|k|)\Delta s] = g\left[(\rho_s - \rho_w)H(k) - (\rho_m - \rho_s) \right.$$

$$\left. \cdot T(k) \right] + \delta(|k|)g\left[(\rho_m - \rho_w)\Delta s - (\rho_s - \rho_w)C_s \right] \qquad (18)$$

By definition, both T and H approach zero as $|k| \rightarrow 0$, therefore the second term on the right side of (18) must be zero for all wavenumbers. The solution to (18) when $|k| = 0$ is

$$\Delta s = \frac{(\rho_s - \rho_w)}{(\rho_m - \rho_w)} C_s \qquad (19)$$

and the average basement depth s' is now

$$s' = s + \frac{(\rho_s - \rho_w)}{(\rho_m - \rho_w)} C_s \qquad (20)$$

A similar equation is commonly used to correct seafloor depths for isostatic loading by sediments. However, the sediment unloading procedure described in (20) is just the very long wavelength approximation to the more complete flexural unloading problem. The terms corresponding to the nonzero wavenumber part of (18) describe the flexural deformation caused by undulations in the sediment thickness. After solving (18) for $T(k)$ we find

$$T(k) = R_2(|k|) \frac{(\rho_s - \rho_w)}{(\rho_m - \rho_s)} H(k) \qquad (21)$$

where

$$R_2(|k|) = \left[1 + \frac{D_2|k|^4}{g(\rho_m - \rho_s)} \right]^{-1} \qquad (22)$$

and the flexural wavelength λ_{f2} now becomes

$$\lambda_{f2} = 2\pi \left[\frac{D_2}{g(\rho_m - \rho_s)} \right]^{1/4} \qquad (23)$$

The basement topography $B(k)$ with respect to the average basement depth s' is $H(k) + T(k)$ or by using (21):

$$B(k) = \left[1 + R_2 \frac{(\rho_s - \rho_w)}{(\rho_m - \rho_s)} \right] H(k) \qquad (24)$$

It is interesting that the basement topography is amplified with respect to the original topography especially for low wavenumbers. After the second deflection the undulations along the Moho are $W(k) + T(k)$.

The gravity anomaly is the sum of the gravity caused by undulations in the sediment/basement interface and the gravity field caused by undulations along the crust/mantle interface:

$$G(k) = 2\pi Ge^{-|k|s'} \left\{ (\rho_c - \rho_s)B(k) \right.$$

$$\left. + e^{-|k|d}(\rho_m - \rho_c)[W(k) + T(k)] \right\} \qquad (25)$$

Using (9), (21), and (24), we express $W + T$ in terms of the basement topography and insert this expression into (25), which yields

$$G(k) = Q_2(|k|) B(k) \qquad (26)$$

TABLE 1. Definitions and Values of Parameters

Parameter	Definition	Value (T53-54)	Value (T6-11)
C_s	mean sediment thickness	7.1 km	4.1 km
d	crustal thickness	6.0 km	6.0 km
D_1	ridge formation flexural rigidity	1.8×10^{21} N m	1.0×10^{21} N m
D_2	sediment loading flexural rigidity	3.2×10^{23} N m	1.8×10^{23} N m
E	Young's modulus	6.5×10^{10} N m^{-2}	6.5×10^{10} N m^{-2}
g	gravitational acceleration	9.82 m s^{-2}	9.82 m s^{-2}
G	gravitational constant	6.5×10^{11} m^3 kg^{-1} s^{-2}	6.5×10^{11} m^3 kg^{-1} s^{-2}
λ_{f1}	ridge formation flexural wavelength	152 km	131 km
λ_{f2}	sediment loading flexural wavelength	471 km	408 km
ρ_w	seawater density	1025 kg m^{-3}	1025 kg m^{-3}
ρ_s	sediment density	2300 kg m^{-3}	2300 kg m^{-3}
ρ_c	crustal density	2800 kg m^{-3}	2800 kg m^{-3}
ρ_m	mantle density	3330 kg m^{-3}	3330 kg m^{-3}
s	seafloor depth corrected for sediment load	6.2 km	5.7 km
s'	average basement depth	10.2 km	8.0 km
σ	Poisson's ratio	0.25	0.25

where Q_2, the gravity/basement topography transfer function, is

$$Q_2(|\mathbf{k}|) = 2\pi G e^{-|\mathbf{k}|s'}\left\{(\rho_c - \rho_s) + e^{-|\mathbf{k}|d}(\rho_m - \rho_c)\right.$$

$$\left.\cdot\left[1 + R_2\frac{(\rho_s - \rho_w)}{(\rho_m - \rho_s)}\right]^{-1}\left[R_2\frac{(\rho_s - \rho_w)}{(\rho_m - \rho_s)} - R_1\frac{(\rho_c - \rho_w)}{(\rho_m - \rho_c)}\right]\right\}$$

(27)

The function R_1 and R_2 contain the flexural rigidities D_1 and D_2, respectively.

Figure 8b shows the gravity/basement topography transfer function for $D_1 = D_2 = 1.8\times10^{21}$ N m (dashed line) and $D_1 = 1.8\times10^{21}$ N m $< D_2 = 3.2\times10^{23}$ N m (solid line). When $D_1 = D_2$, the transfer function (dashed line) is positive for all wavelengths. However, when $D_2 > D_1$, the transfer function is negative for wavelengths $\lambda > \lambda_{f1}$. Thus the negative gravity/basement topography ratio is a consequence of an increase in flexural rigidity between the time of ridge formation and the time of sediment burial.

This result is not intuitively obvious except in one extreme case. Consider a ridge that was formed on a lithosphere with zero flexural rigidity (i.e., Airy compensated). The gravity field is composed of a large positive field from the topography and a large negative field from its root. The overall gravity measured on the sea surface is slightly positive since the observer lies closer to the positive mass than the low density root. Suppose further that the lithospheric flexural rigidity is increased to infinity prior to sediment loading. In this case the lithosphere does not flex under the sediment load, and the negative gravity field from the root remains unchanged. However, the seawater has been displaced by sediments, which lowers the density contrast from $(\rho_c - \rho_w)$ to $(\rho_c - \rho_s)$.

This also lowers the positive gravity field by the same factor. The total gravity field measured on the sea surface is now strongly negative and reflects the undulations along the Moho. While this is an extreme case, the same effect can occur whenever the flexural rigidity of the lithosphere increases between the two loading events.

Results

In this section we use the basement topography models T53-54 and T6-11 (Figures 4 and 5) with our two-stage loading model to reproduce the observed gravity anomalies along these two profiles. Based upon the isopach map (Figure 2) and the free-air gravity anomaly map (Figure 3), it appears that the length of the 85°E Ridge is about 10 times greater than its width. Therefore we approximate the basement topography $b(x)$ as an infinitely long ridge in the $\hat{y}$ direction with an amplitude that varies in the $\hat{x}$ direction according to the basement models. The gravity anomaly is calculated by taking the digital Fourier transform of the basement topography, multiplying by the transfer function Q_2, equation (27), and inverse transforming the result [see McKenzie and Bowin, 1976]. The transfer function Q_2 contains a number of model parameters whose values range from unknown to well known as follows: unknown (D_1 and D_2), reasonably well known (d, ρ_s, ρ_c, and ρ_m), and well known (s', ρ_w, g, and G).

Our goal is to match the two observed gravity profiles by varying the model parameters. Clearly, both the errors in the seismically determined basement topography and the errors introduced by modeling assumptions will have an effect upon the 'best set' of model parameters. To estimate the sensitivity of the model gravity field to the model parameters, we chose a reasonable set of starting model parameters (D_1, D_2, d, ρ_s, ρ_c, ρ_m). The values of these parameters are given in Table 1. We then varied each of the parameters, within reasonable bounds, while holding the others constant. For instance, we varied the crustal density between 2700 and 2900 kg/m^3. However, this

variation in ρ_c changes the model gravity field by only a few milligals. Similarly, the model gravity field is insensitive to reasonable variations in ρ_m, ρ_s, and d. This insensitivity is built into the model. For example, (9) shows that a crustal density increase is compensated by an increase in undulation amplitude along the crust-mantle boundary. On the other hand, reasonable variations in D_1 and D_2 (i.e., 10^{20} to 10^{24} N m) produce large variations in the model gravity field.

This sensitivity analysis demonstrates that we will be able to place constraints on the values of D_1 and D_2 but cannot improve the already tight constraints on the values

Fig. 10. (a) A comparison between the observed free-air gravity profile (solid line) and the predicted anomaly for the best model (dashed line). The dotted line is the difference between them. The data outside of the region marked by arrows were not used in the rms misfit calculation. (b) Model of crustal structure.
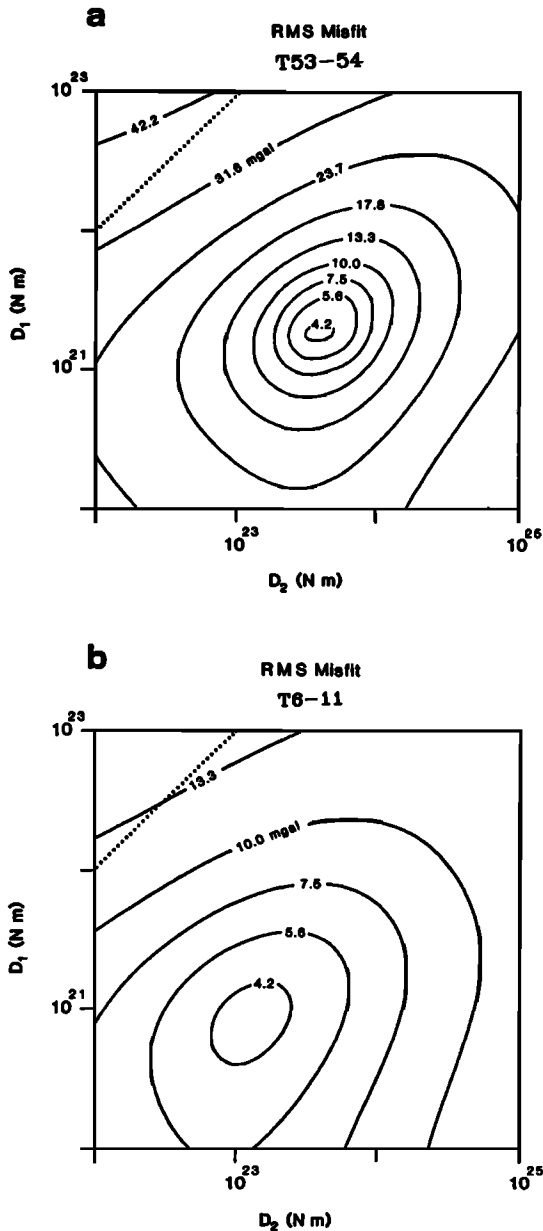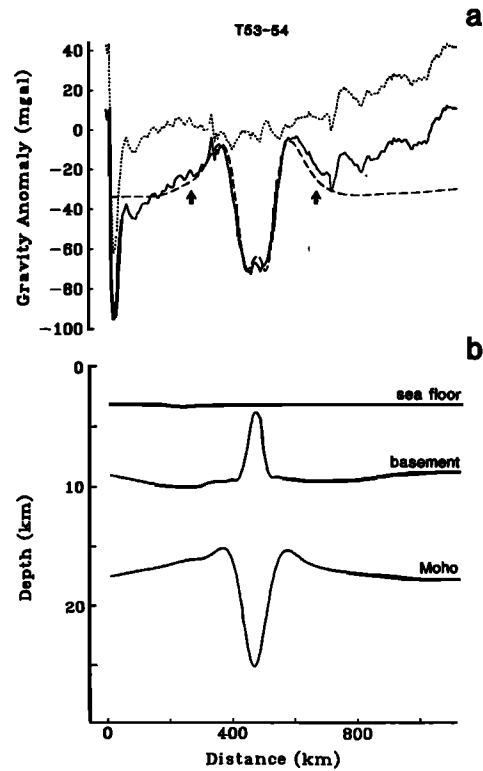
Fig. 9. (a) Contours of the root mean square (rms) misfit between the model (± a constant) and the data for various values of initial flexural rigidity D_1 and final flexural rigidity D_2 (logarithmic scale). The smallest misfit occurs when $D_1 = 1.8 \times 10^{21}$ N m and $D_2 = 3.2 \times 10^{23}$ N m. The dotted line indicates where $D_1 = D_2$. (b) Contours of rms fit for gravity profile T6-11. The minimum misfit value ~4 mGal occurs when $D_1 = 1 \times 10^{21}$ N m and $D_2 = 1.8 \times 10^{23}$ N m.

of ρ_s, ρ_c, ρ_m, and d. Moreover, the 'best set' of D_1 and D_2 values will be insensitive to the assumed values of the other parameters. The value of sediment density is the most poorly constrained of all the densities. When the sediment cover is less than a few hundred meters, this density may be as low as 1700 km/m³, which is based upon a seismic velocity of 2 km/s [Sclater et al., 1975]. However, adjacent to the 85°E Ridge the sediment thickness exceeds a few kilometers, indicating that it is highly compacted because of the large overburden pressure. The flat sediments, lying above the crest of the 85°E Ridge, have no effect upon the undulations in the gravity field. To assign a density to the deeper sediments, we use a velocity/density relationship [Ludwig et al., 1970]. The sediment velocities adjacent to the 85°E Ridge vary from 3.0 to 5.0 km/s. This corresponds to densities ranging from 2200 to 2400 kg/m³. For our modelling we chose an average value of 2300 kg/m³.

We have estimated the ranges of acceptable D_1 and D_2 values for each profile by calculating model gravity profiles for $10^{20} < D_1 < 10^{23}$ N m and $10^{22} < D_2 < 10^{25}$ N m, and comparing these models to the observed profiles. The measure of misfit was assumed to be the root mean square (rms) of the difference between the model (plus or minus a constant) and the data, over a distance of 200 km on either side of the 85°E Ridge. Contours of rms misfit in milligals are presented in Figure 9 as a function of D_1 and D_2. For profile T53-54, the smallest misfit, 4.2 mGal, occurs at $D_1 = 1.8 \times 10^{21}$ N m and $D_2 = 3.2 \times 10^{23}$ N m, which lies well below the dotted line $D_1 = D_2$ (Figure 9a).
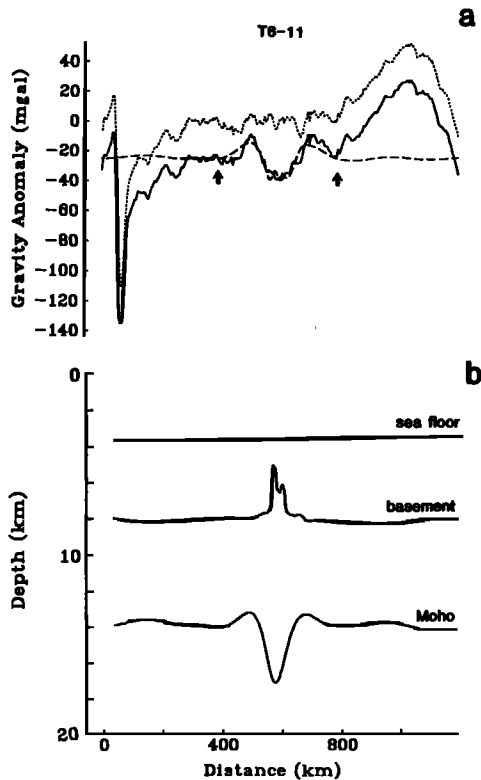
Fig. 11. (a) Observed gravity profile (solid line), best model profile (dashed line), and their differences (dotted line) for profile T6-11. (b) Model of crustal structure.

In every direction away from the minimum, the misfit increases rapidly. Thus the values of D_1 and D_2 are well constrained by the data, although there is no statistical basis for defining an unacceptable misfit. The model profile corresponding to this best set of D_1 and D_2 values is shown in Figure 10a (dashed line), along with the observed gravity profile (solid line) and the difference between them (dotted line). The arrows indicate the portion of the profile that was used to calculate the misfit. Within this region the agreement between the model and the data is quite good. The model correctly predicts the overall gravity low and the surrounding relative gravity highs. Furthermore, the model matches the small bump on the most negative portion of the observed profile. Ths agreement is not coincidental. If the value of D_1 is raised above 1.8×10^{21} N m, then the amplitude of the small bump increases; when $D_1 = D_2$, this bump dominates, and the entire model gravity field is positive relative to surrounding values. Similarly, if D_1 is lowered, the model gravity low deepens.

The structural model producing this gravity field is shown in Figure 10b. The Moho undulations were calculated from the basement model through (24), (21), and (9). A comparsion of Figures 10a and 10b reveals that the gravity field is dominated by the undulations along the Moho. This occurs because the Moho has larger undulations and is associated with a larger density contrast than the basement. The downwarping of the Moho immediately beneath the ridge is produced by ridge formation on a weak lithosphere. The upwarping of the Moho adjacent to the deep root occurs during sediment burial when the

ridge and its root became buoyant with respect to the surrounding crust. Our model predicts a similar upwarping of the basement topography adjacent to the ridge. However, with so few basement depth samples it is impossible to detect this effect.

Figure 11 shows comparable results for profile T6-11. Along this track the amplitude of both the 85°E Ridge and its negative gravity field are relatively low. Because of this weaker signal, the values of D_1 and D_2 are not as well constrained as those for profile T53-54. The smallest misfit for T6-11 occurs at $D_1 = 1 \times 10^{21}$ N m and $D_2 = 1.8 \times 10^{23}$ N m (Figure 9b). These values are approximately a factor of 2 lower than the respective values for profile T53-54. Again, the best fitting models have values of D_2 that are greater than D_1.

For both profiles the lithospheric flexural rigidity increased by a factor of about 180 between the time of ridge formation and the time of sediment loading. Before discussing these results, we must demonstrate that these best sets of D_1 and D_2 values are not highly dependent upon the more speculative portions of the basement models. Along basement profile T53-54, in Figure 4, the width of the ridge was not constrained by any data but instead was inferred from the shape of the overlying unconformities and the width of the magnetic signature. It could possibly be much narrower than the value we assumed but probably not much wider (i.e., more than a factor of 2 wider). To test the effects of a narrower ridge, we recalculated the gravity model by using a Gaussian-shaped ridge with a half width of 10 km and an amplitude of 10 km. This very narrow ridge is close to a delta function source but does not significantly alias the fast Fourier transform. The gravity model for this ridge, which was calculated using the best T53-54 D_1 and D_2 values, is shown in Figure 12. The fit is suprisingly good (rms misfit of 10 mGal). The amplitude and characteristic width of the model gravity profile are close to the observed profile. The largest discrepancy occurs at the peak within the gravity low, which is much greater in the model profile than it is in the observed profile. These calculations demonstrate that the width of the model gravity field is controlled by the value of D_2 and not the width of
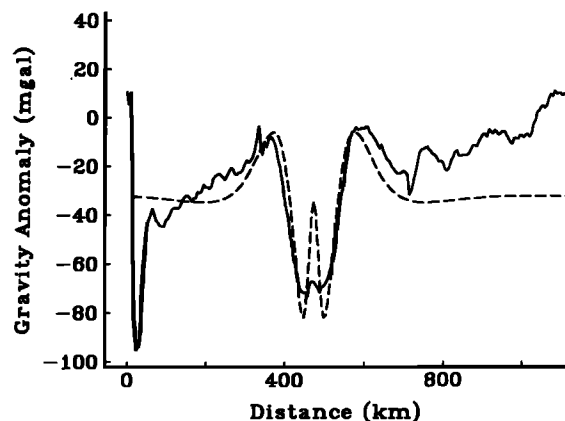

Fig. 12. The gravitational response of the model (dashed line) to a narrow Gaussian-shaped ridge (half width 10 km) is compared with the observed gravity anomaly along profile T53-54 to demonstrate the insensitivity of the gravity field to the ridge width.

the basement model. Thus the gravity profiles along T53-54 and T6-11 are close to the impulse response gravity profiles and depend mainly upon the source location, the source amplitude, and the properties of the earth. This rather fortunate situation allows us to examine the rheological properties of the earth without an accurate knowledge of the source (i.e., the shape of the ridge).

DISCUSSION

The best set of D_1 and D_2 values can be used to estimate the times of the two loading events, since the first-order relationship between flexural rigidity and age is fairly well understood [*Watts*, 1978; *Bodine et al.*, 1981]. *Caldwell and Turcotte* [1979] have presented an effective elastic thickness versus age relation that is based upon flexure studies of large seamounts and subduction zones and also upon a theoretical thermomechanical model of the oceanic lithosphere. Recently, *McNutt and Menard* [1982] have demonstrated that the EET's derived from purely elastic models tend to be underestimates of the true EET, when bending stresses exceed the yield envelope. However, the stresses inferred from seamount flexure studies are generally within the yield envelope (i.e. the stress-strain relationship is linear). Accordingly, we neglect the nonlinear effects and interpret the changes in flexural rigidity using the theoretical EET-age relationship [*Caldwell and Turcotte*, 1979, curve 1, Figure 3]. The relationship between effective elastic thickness h_e and flexural rigidity D, given by *Love* [1906, p. 443]:

$$D = Eh_e^3 / [12(1 - \sigma^2)]$$

is used to calculate EET values from our D_1 and D_2 estimates, where the values of Young's modulus E and Poisson's ratio σ are the same as the values used by *Caldwell and Turcotte* [1979]. The EET's for D_1 and D_2 of T53-54 are 6.8 and 38.1 km, respectively, corresponding to ages of 10.9 and 68.9 m.y. The EET's for profile T6-11 are slightly lower, 5.6 and 35.1 km, corresponding to ages of 9.6 and 51.1 m.y. for D_1 and D_2, respectively.

Before trying to make inferences about tectonic processes from the ages derived from the D_1 and D_2 values, we should point out the large degree of scatter in the observed flexural rigidity-age relationship. Some of this scatter is associated with the nonlinear flexural response of the lithosphere [*McNutt and Menard*, 1982]. In any case, the scatter in the EET-age relationship introduces large errors in our estimates of the age of the lithosphere at the time of ridge formation (uncertainty ±5 m.y.) and larger errors at the time of sediment loading (uncertainty ±10-20 m.y.).

Considering all of the uncertainties, we conclude that the 85°E Ridge was formed on young (10 ± 5 m.y.), hot lithosphere that flexed readily under the load of the ridge. Sediment burial may have begun immediately following ridge formation. However, most of the 85°E Ridge was buried when the lithosphere was 40-80 m.y. old. This scenario is consistent with plate reconstruction models [*Curray and Moore*, 1974; *Johnson et al.*, 1976; *Norton and Sclater*, 1979; *Curray et al.*, 1982], which show that the formation of the eastern Indian Ocean occurred after India

separated from Australia and Antarctica. Identified magnetic anomalies off the northwest coast of Australia indicate that this breakup started earlier than 127 m.y. ago [*Markl*, 1974, 1978; *Larson*, 1977]. Reconstruction models predict that the crust in the northwestern portion of the Bay of Bengal has a similar age (~130 m.y.). According to these models, the central portion of the Bay of Bengal (i.e., location of T53-54 and T6-11 in the vicinity of the 85°E Ridge) is somewhat younger (100-120 m.y. old), with the older seafloor lying to the northwest. Figures 4 and 5 show that the 85°E Ridge was almost completely buried at the end of the Paleocene, or about 55 m.y. B.P. Thus the lithosphere was approximately 65 m.y. old by the time the ridge was completely buried. This is compatible with our estimate of 40-80 m.y. for the average age of the lithosphere during sediment loading. Moreover, our model predicts that the lithosphere at the time of sediment loading was younger along T6-11 than T53-54. This is also in agreement with the plate reconstruction models if both portions of the ridge were buried during the same period of time (i.e., when the Bengal Deep-Sea Fan formed).

Age and mode of origin of the 85°E Ridge had not been postulated in previous studies. The Ninetyeast Ridge, on the other hand, has been attributed to trace of the Kerguelen-Heard hot spot [*Curray and Moore*, 1974; *Curray et al.*, 1979, 1982]. Inasmuch as these two ridges are not parallel but instead appear to diverge rather markedly, it is unlikely that they were both formed on the same plate as it passed over two distinct hot spots, unless the hot spots have moved relative to each other or the plate has rotated significantly. Other possible modes of origin are difficult to conceive but can now be constrained by the conclusions of this study.

CONCLUSIONS

1. The 85°E Ridge is similar in many respects to other aseismic ridges; it has an amplitude of up to 6 km, a length of approximately 1600 km, and a strong magnetic signature.

2. The major differences between this ridge and other aseismic ridges are that it is completely buried by a thick layer of sediments and it has a negative free-air gravity anomaly over the crest of the ridge.

3. We have used a simple two-stage loading model to demonstrate that the negative gravity anomaly over the 85°E Ridge is a direct consequence of sediment loading and that the flexural rigidity of the lithosphere when the ridge was formed was about 180 times less than the flexural rigidity of the lithosphere during the sediment loading.

4. Using an approximate relationship between flexural rigidity and age we find that the sediment loading age is in agreement with the interpreted ages of the adjacent and covering sediments and the plate reconstruction models. We have also determined that the 85°E Ridge was formed on young (about 10 m.y.), hot lithosphere with low rigidity.

5. We suggest that the alteration of the gravity field by a thick layer of sediments may occur in other large sedimentary basins or along continental margins.

REFERENCES

Banks, R. J., R. L. Parker, and J. P. Heustis, Isostatic compensation on a continental scale: Local versus regional mechanisms, *Geophys. J. R. Astron. Soc., 51,* 431-452, 1977.

Bodine, J. H., M. S. Steckler, and A. B. Watts, Observations of flexure and the rheology of the oceanic lithosphere, *J. Geophys. Res., 86,* 3695-3707, 1981.

Bowin, C., Origin of the Ninety East Ridge from studies near the equator, *J. Geophys. Res., 78,* 6029-6043, 1973.

Caldwell, J. G., and D. L. Turcotte, Dependence of the thickness of the elastic oceanic lithosphere on age, *J. Geophys. Res., 84,* 7572-7576, 1979.

Curray, J. R., and D. G. Moore, Growth of the Bengal deep-sea fan and denudation in the Himalayas, *Geol. Soc. Am. Bull., 82,* 563-572, 1971.

Curray, J. R., and D. G. Moore, Sedimentary and tectonic processes in the Bengal deep-sea fan and geosyncline, in *The Geology of Continental Margins,* edited by C. A. Burk and C. L. Drake, pp. 617-628, Springer-Verlag, New York, 1974.

Curray, J. R., D. G. Moore, and F. J. Emmel, The northern end and geologic history of the Ninetyeast Ridge, *Geol. Soc. Am. Annual Meeting Abst. with Programs,* p. 408, 1979.

Curray, J. R., F. J. Emmel, D. G. Moore, and R. W. Raitt, Structure and tectonics of the northeastern Indian Ocean, in *The Ocean Basin and Margins,* Vol. 6, *The Indian Ocean,* edited by A. E. M. Nairn and F. G. Stehli, pp. 399-450, Plenum, New York, 1982.

Detrick, R., and A. B. Watts, An analysis of isostasy in the world's oceans, 3, Aseismic ridges, *J. Geophys. Res., 84,* 3637-3653, 1979.

Dorman, L. M., and B. T. R. Lewis, The use of nonlinear functional expansions in calculation of the terrain effect in airborne and marine gravimetry and gradiometry, *Geophysics, 39,* 33-38, 1974.

Goslin, J., and J. C. Sibuet, Geophysical study of the easternmost Walvis Ridge, South Atlantic: Deep structure, *Geol. Soc. Am. Bull., 86,* 1713-1724, 1975.

Gunn, R., A quantitative study of isobaric equilibrium and gravity anomalies in the Hawaiian Island, *J. Franklin Inst., 236,* 373-390, 1943.

Heiskanen, W. A., and F. A. Vening Meinesz, *The Earth and Its Gravity Field,* McGraw-Hill, New York, 1958.

Johnson, B. D., C. M. Powell, and J. J. Veevers, Spreading history of the eastern Indian Ocean and Greater India's northward flight from Antarctica and Australia, *Geol. Soc. Am. Bull., 87,* 1560-1566, 1976.

Kogan, M. G., The gravity field of oceanic block ridges, *Izv. Acad. Sci. USSR Phys. Solid Earth, 12,* 710-717, 1976.

Larson, R. L., Early Cretaceous breakup of Gondwanaland off western Australia, *Geology, 5,* 57-60, 1977.

Lerch, F. J., S. M. Klosko, R. E. Laubscher, and C. A. Wagner, Gravity model improvement using Geos 3 (GEM 9 and 10), *J.*

Geophys. Res., 84, 3897-3916, 1979.

Love, A. E. H., *A Treatise on the Mathematical Theory of Elasticity,* 2nd ed., Cambridge University Press, London, 1906.

Ludwig, W. J., J. E. Nafe, and C. L. Drake, Seismic refraction, in *The Sea,* Vol. 4, Part I, edited by A. E. Maxwell, 53-84, Wiley-Interscience, New York, 1971.

Markl, R. I., Evidence for breakup of eastern Gondwanaland by the early Cretaceous, *Nature, 251,* 196-200, 1974.

Markl, R. I., Further evidence for the early Cretaceous breakup of Gondwanaland off southwestern Australia, *Mar. Geol., 26,* 41-48, 1978.

McKenzie, D., and C. Bowin, The relationship between bathymetry and gravity in the Atlantic Ocean, *J. Geophys. Res., 81,* 1903-1915, 1976.

McKenzie, D., and J. G. Sclater, The evolution of the Indian Ocean since the Late Cretaceous, *Geophys. J. R. Astron. Soc., 25,* 437-528, 1971.

McNutt, M. K., and H. W. Menard, Constraints on yield strength in the oceanic lithosphere derived from observations of flexure, *J. Geophys. Res.,* in press, 1982.

Moore, D. G., J. R. Curray, R. W. Raitt, and F. J. Emmel, Stratigraphic-seismic section correlations and implications to Bengal Fan history, *Initial Rep. Deep Sea Drill. Proj., 22,* 403-412, 1974.

Norton, I. O., and J. G. Sclater, A model for the evolution of the Indian Ocean and the break up of Gondwanaland, *J. Geophys. Res., 84,* 6803-6830, 1979.

Parker, R. L., The rapid calculation of potential anomalies, *Geophys. J. R. Astron. Soc., 31,* 447-455, 1973.

Schouten, H., and K. McCamy, Filtering marine magnetic anomalies, *J. Geophys. Res., 77,* 7089-7099, 1972.

Schouten, J. A., A fundamental analysis of magnetic anomalies over oceanic ridges, *Mar. Geophys. Res., 1,* 111-144, 1971.

Sclater, J. G., L. A. Lawver, and B. Parsons, Comparison of long-wavelength residual elevation and free air gravity anomalies in the north Atlantic and possible implications for the thickness of the lithosphere, *J. Geophys. Res., 80,* 1031-1053, 1975.

Turcotte, D. L., Flexure, *Adv. Geophys., 21,* 51-86, 1979.

Vening Meinesz, F. A., Gravity over the Hawaiian Archipelago and over the Madeira area: conclusions about the earth's crust, *Proc. K. Ned. Akad. Wetensch., 44,* 1-12, 1941.

Walcott, R. I., Flexure of the lithosphere at Hawaii, *Tectonophysics, 9,* 435-446, 1970.

Walcott, R. I., Gravity, flexure, and the growth of sedimentary basins at a continental edge, *Geol. Soc. Am. Bull., 83,* 1845-1848, 1972.

Watts, A. B., An analysis of isostasy in the world's ocean, 1, Hawaiian-Emperor seamount chain, *J. Geophys. Res., 83,* 5989-6004, 1978.

Watts, A. B., and J. R. Cochran, Gravity anomalies and flexure of the lithosphere along the Hawaiian-Emperor seamount chain, *Geophys. J. R. Astron. Soc., 38,* 119-141, 1974.

Watts, A. B., and M. Talwani, Gravity anomalies seaward of deep-sea trenches and their tectonic implications, *Geophys. J. R. Astron. Soc., 36,* 57-90, 1974.